MATERIALS CHEMISTRY FRONTIERS

RESEARCH ARTICLE

View Article Online
View Journal | View Issue

Cite this: *Mater. Chem. Front.*, 2023, 7, 4908

Photostabilisation of an omniphobic, drop-castable surface coating by transformation of a self-assembled supramolecular xerogel into a covalent polymer xerogel†

Janos Wasternack, Tom White, Sebastian Müller and Christoph A. Schalley *

Received 3rd May 2023,
Accepted 3rd August 2023

DOI: 10.1039/d3qm00506b

rsc.li/frontiers-materials

Simple drop-casting of a new gelator, incorporating a diacetylene core and fluorous ponytails, yields porous xerogels as surface coatings. The mechanical stability of such coatings is quantified with a self-devised scratch balance, introducing a simple and universal quantification method to compare the stability of μm-scale coatings. The diameters of the pores in the coatings can be controlled by the breath figure effect. The coatings display omniphobicity with static contact angles of up to 139° (water) and 96° (*n*-decane). The coatings are topochemically polymerised by UV irradiation, enhancing the mechanical stability by up to four times. Simultaneously, the water and *n*-decane contact angles are increased by about 9° and 4° respectively due to a slight increase in surface roughness.

1. Introduction

The water-repellent properties of natural materials like the lotus leaf or monks cress surfaces are well known as the "lotus effect". Water droplets adhere very little to these leaves and thus simply roll off their surface. Rose petals, in contrast, also display hydrophobicity, yet the droplets do not roll off their leaves but adhere to the surface. Surfaces with high contact angles and high tilt angles and contact angle hysteresis display the "rose petal effect". The different behaviour is caused by the wetting mode at the liquid–solid–gas interface: Lotus-like surfaces display Cassie–Baxter wetting, whereby the droplet sits on top of an air pocket, which is constrained within high, pillar-like structures. In contrast, the structures on rose-like surfaces are shorter, which allows liquids to penetrate the space between them (Wenzel wetting), thus pinning droplets onto the surface.[1,2]

Inspired by the nano-micro-structures of natural hydrophobic surfaces, many biomimetic hydro- as well as lipophobic coatings have been developed.[3,4] Such omniphobic (*i.e.* hydro- and oleophobic) coatings are widely applied in industry, households and medicine.[5,6] Among the most prominent applications, omniphobic PTFE-coated frying pans are found in most households; hydrophobic paints for cars or buildings save labour and minimise the introduction of detergents into the environment; and medical instruments with omniphobic properties are more germ-resistant.[7]

These highly omniphobic surfaces are obtained through a combination of two critical aspects: firstly, the surface material should display "orthogonal" phase properties, *i.e.* little to no attractive intermolecular forces should exist between the solid surface and the applied liquid. Secondly, appropriate structuring of the surface should be employed by increasing the surface roughness, thus lowering the surface energy.[8,9]

Regarding the first aspect, hydrophobic surfaces can thus either be made from oleophilic or fluorous materials, while oleophobic surfaces are best made from fluorous materials. The most prominent hydrophobic and oil-repelling material is PTFE with a static water contact angle of $^{H_2O}CA = 118°$[10] and an *n*-decane contact angle of $^{dec}CA = 35°$.[11] Much higher contact angles ^{H_2O}CA of up to 165° are observed on superhydrophobic lotus leaves[1] indicating that besides the material another important factor must be present: the roughness caused by a hierarchical nano- and micrometer-sized structuring of the surface. Entrapped air pockets limit the contact area between the solid phase and the liquid phase which sits on top of the roughness protrusions.[8,12]

Various techniques have been used to create such structured surfaces, including etching, laser ablation, vapour deposition, dip coating, spin coating, deposition of self-assembled monolayers or drop casting.[5,8,13] Each of these methodologies provides its own advantages and disadvantages: post-structuring usually allows the manufacture of mechanically robust surfaces, as the structure is imparted into a homogeneous matrix, whereas coatings rely on strong interactions between the coating and the substrate to achieve similar mechanical stabilities.[14] Post-structuring methods need to be suitable for the chosen material, whereas coatings can be applied to a broad range of different substrates.[15,16]

Institut für Chemie und Biochemie, Freie Universität Berlin, Arnimallee 20, 14195, Berlin, Germany. E-mail: c.schalley@fu-berlin.de

† Electronic supplementary information (ESI) available: Synthetic procedures and surface characterisation methods. See DOI: https://doi.org/10.1039/d3qm00506b

Among coating methods, drop casting is particularly convenient, as no special equipment is needed for the application. We previously demonstrated that superhydrophobic lotus-like coatings can be prepared by this method.[17,18] The present study aims to transfer this approach to rose-petal like coatings. In both cases, the surface roughness can be obtained by drop-casting of a suitable fluorous low molecular weight gelator (LMWG) solution, which self-assembles into a supramolecular polymer gel that becomes a structured xerogel upon drying.[17–20] A rather complex surface structure can thus be obtained conveniently by drop-casting of a suitable self-assembling gelator.[20]

As the mechanical stability of such coatings is determined by the cohesive forces within the xerogel network, which in the case of LMWGs are non-covalent interactions, the mechanical stability of such coatings often lags behind that of covalent polymeric coatings. Enhancing the mechanical stability of supramolecular polymers is of high interest for the application of supramolecular coatings.[21–23]

Herein, we report an LMWG (Fig. 1a) which can be photopolymerised in the xerogel state, transforming the formerly hydrogen-bonded supramolecular polymer into a covalent polymer (Fig. 1b). A suitable molecular unit which undergoes such topochemical polymerisation and has been extensively investigated in various other contexts in the past decades is the diacetylene motif.[24–29]

Diacetylene polymerisation to form the strongly coloured polydiacetylenes (PDA) has been described in the crystalline[25,30] as well as in the gel state.[24,27] The required alignment of the diacetylene units is often achieved through non-covalent interactions like hydrogen bonding.[27] Conveniently, the incorporation of multiple H-bonding sites into the molecular design of diacetylenes frequently provides excellent preconditions for gelation and thus, various diacetylene-based gelators have been investigated.[31–33] The polymerisation of diacetylenes is commonly initiated by UV irradiation.[25,34] Although the structural changes during the polymerization process are usually small, the polymerisation is accompanied by a slight contraction of the bulk material which sometimes results in mechanical stress in the solid that can lead to cracking.[35–39] Fig. 1a depicts a fluorous LMWG design on the basis of the well-established diacetylene-diamide gelator motif.[31–33] The central diacetylene-diamide enables self-assembly to cause gelation, simultaneously providing the structural requirements for topochemical polymerisation. The flexible alkyl ester spacers ensure sufficient solubility. The alkyl-extended fluorous ponytails provide a high degree of fluorousness, while maintaining the reactivity of non-fluorous carboxylic acids. As perfluorocarboxylic acids turned out to be rather sensitive to hydrolysis, due to the highly electron-withdrawing nature of fluorocarbons, carboxylic acids with three methylene units between the carboxyl group and the perfluorocarbon chain were used as ponytails here.[40–43]

As an additional means of influencing the surface morphology, the breath figure effect is employed to create porous coatings with different average pore sizes by drop casting LMWG solutions in environments of different relative humidity (RH).[44–47] Topochemical hardening of the dried coatings is initiated by UV-irradiation.

To quantitatively assess the impact of the surface structuring and the topochemical hardening on the mechanical robustness of the coatings, a methodology and suitable equipment were devised.

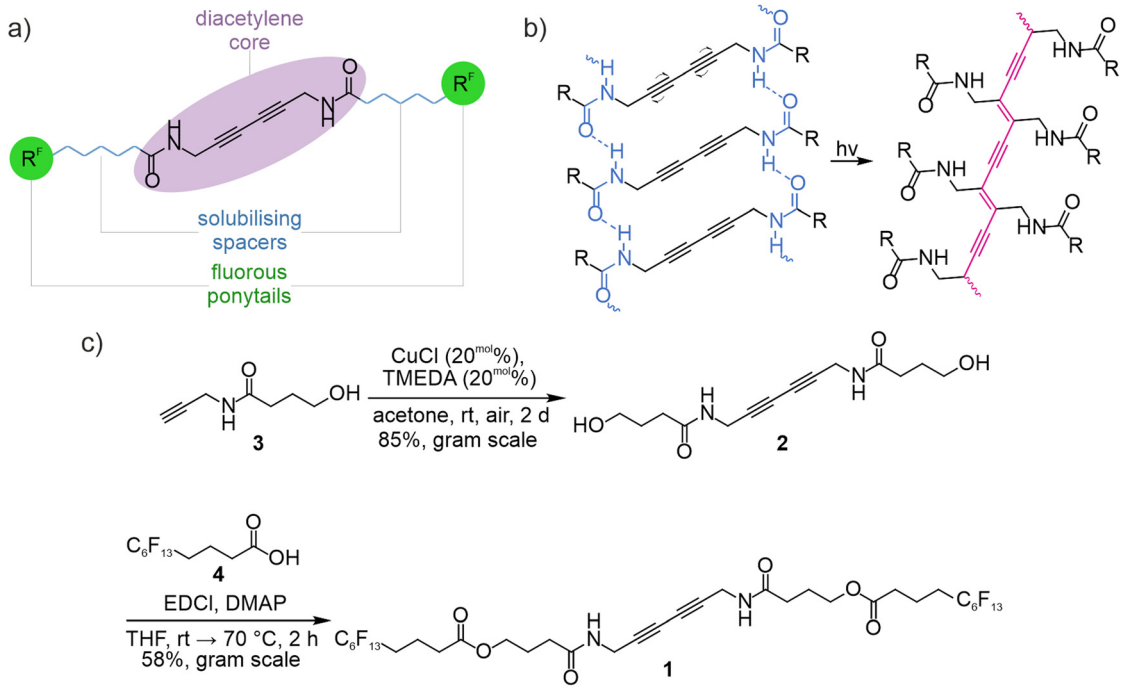

Fig. 1 (a) Molecular building blocks of diacetylene-based, fluorous LMWG. (b) Topochemical polymerisation of diacetylenes can only occur if they are preorganised into the required structural arrangement.[28] (c) Synthesis of fluorous LMWG **1**. Literature-known acetylene **3** is dimerised by HAY-coupling forming diacetylene **2** and the ponytails are subsequently attached by STEGLICH-esterification with fluorous carboxylic acid **4**.

2. Results and discussion

2.1. Coating preparation and morphological analysis

2.1.1. Synthesis of LMWG 1. Diacetylene **1** is synthesised as shown in Fig. 1c. Literature-known alcohol **3**[48,49] is dimerised by HAY-coupling[50,51] to form diacetylene **2**. STEGLICH esterification of carboxylic acid **4** with diacetylene **2** provides diacetylene **1** in 58% yield. Alternatively, diacetylene **1** can be obtained by esterification of alcohol **3** with carboxylic acid **4** and subsequent HAY-coupling, however this sequence is less favourable due to the low yields of the HAY-coupling and the necessity of carrying the expensive fluorous ponytail through two reactions instead of introducing it in the final step.

2.1.2. Drop-casting of supramolecular gel coatings. To ensure the evenness of the xerogel and to avoid the Marangoni and coffee ring effects, the solvent containing the gelator is evaporated slowly allowing progressive gelation. The structured morphology of the supramolecular gel is retained by the xerogel.[52]

Different solvents have been investigated with respect to their capability to support gelation[17,20,53] of LMWG **1** as well as the morphology resulting from drop casting of LMWG **1**. Diacetylene **1** is an efficient LMWG in toluene, chloroform, mixtures of chloroform and cyclohexane, diethyl ether and trifluoromethyl benzene (Fig. 2e). As the solubility of diacetylene **1** in chloroform is rather high, a higher concentration of 50 mg mL^{-1} is required, whereas the other solvents form gels already at 10 mg mL^{-1}.

An appropriate amount of coating needs to be applied to a given surface area to ensure even coverage: deposition of a lower amount per area, either by casting the same volume of a more dilute solution or by application of a smaller volume of the same, more concentrated solution, does not generally lead to thinner coatings. Rather, driven by the self-assembly and subsequent gelation, non-uniform coverage of the substrate results from the use of too little material. The coating frequently becomes thicker on the edges with too dilute LMWG solutions (due to late gelation), or the solution does not cover the whole substrate in the first place if too little volume is used in relation to the surface area of the substrate.

Some solvents of low miscibility with water and high heats of evaporation, most commonly chloroform, lead to the occurrence of the breath figure effect.[54–57] The resulting breath figure patterns contribute to the micro-structure of the coatings and increase their uniformity. As the pore-size of the breath figures is determined by the RH and temperature of the surrounding atmosphere, concentration, temperature and solvent evaporation rates need to be precisely controlled. Thus, drop casting and subsequent drying has been performed within a climate chamber with controlled RH at room temperature (Fig. S1, ESI†).

Optical microscopy of the coatings reveals the impact of the above factors on the coating morphology (Fig. S2, ESI†): Smooth coatings with a moderate $^{H_2O}CA = 125^\circ$ are obtained by drop casting a hot solution of LMWG **1** in trifluoromethyl benzene. Some crystals are embedded within the amorphous matrix of the coating. However, as these did not protrude through the surface of the coating, no additional roughness results from their presence. In contrast, a hot toluene solution results in the deposition of LMWG **1** as fine crystalline powder, displaying higher $^{H_2O}CA = 135^\circ$, but providing no mechanical stability. Coatings deposited from diethyl ether exhibit contact angles as high as $^{H_2O}CA = 161^\circ$ and thus may be considered superhydrophobic. However, these coatings are rather irregular, and their mechanical stability is impaired by rather extensive cracking. Coatings from dichloromethane are quite unevenly distributed and show small contact angles of $^{H_2O}CA = 116^\circ$. The most uniform and crack-free coatings are obtained from chloroform with $^{H_2O}CA = 141^\circ$. Regular arrays of pores caused by the breath figure effect are observed. Because of the regular structure and uniform distribution of the coatings, the coatings obtained from chloroform were chosen for a further investigation of their photopolymerisability. Optimal coverage is obtained by casting of 5 mg per slide. It was reported by Avinash *et al.* that pore size can influence the hydrophobicity of a surface.[44] To obtain coatings with different pore sizes, the deposition was performed with different RH and varying concentrations of LMWG **1**. Coatings with average pore sizes of 7 ± 1 μm, 12 ± 2 μm and 20 ± 4 μm can be created by drop casting of a solution of LMWG **1** (c = 16.7 mg mL^{-1}) in RH = 71%, RH = 81% and RH = 99% respectively. Coatings with a larger average pore size of 30 ± 4 μm are obtained in RH = 99% using a more dilute solution of LMWG **1** (c = 12.5 mg mL^{-1}) (Fig. 2a–d and f).

2.2. Photoaltered properties of diacetylene coatings

2.2.1. Photoinitiated polymerisation of the dried coatings. Coatings of the native, colourless diacetylene **1** polymerise slowly under ambient conditions and quickly by UV (254 nm) irradiation for 1 min to form a red, covalently linked polydiacetylene (PDA) (Fig. 3a). The UV-Vis-spectrum of the native and polymerised materials are shown in 3b. The typical absorption band at 585 nm confirms the formation of PDA.[36] The success of the polymerisation is evident from the typical red colour of PDA's which the coatings display (Fig. 3a). The pore diameters of the irradiated coatings deviate only by 0.7 ± 0.3 μm indicating that the polymerisation has very little influence on the morphology of the coating (Fig. 3e).

2.2.2. Omniphobicity of the coatings. The water and *n*-decane contact angles of native and polymerised coatings are summarised in Fig. 3c and d. With $^{H_2O}CA = 131 \pm 2^\circ$ and $^{dec}CA = 88 \pm 1^\circ$, the native coating can be considered omniphobic. Surprisingly, the breath figure effect has no obvious influence on the hydro- and lipophobicity of the coatings.[44] Irradiation of the coatings leads to a significant increase in both water and *n*-decane contact angles (Fig. 3c and d) by 8° and 4° on average, respectively. This increase likely results from increased surface roughness, which can be observed in the form of little cracks, which form during the polymerisation due to material shrinkage (Fig. 3e).[36] These newly formed cracks appear mostly between pores of the breath figure array. Since these minor cracks do not create gaps within the coatings – as observed for coatings from diethyl ether (Fig. S2, ESI†) – their mechanical integrity is well preserved, while the increase in roughness provides superior omniphobicity. When a coated and irradiated

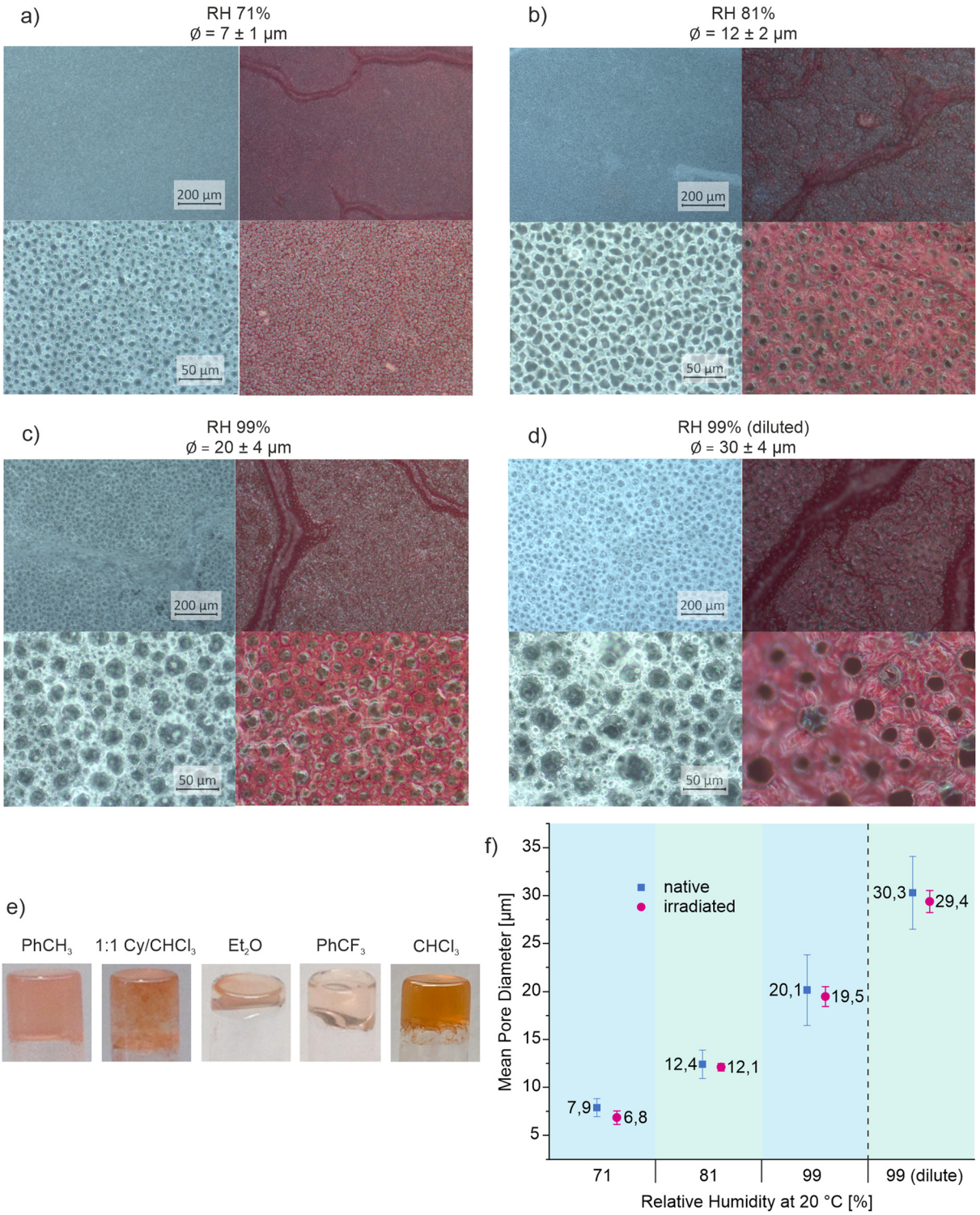

Fig. 2 (a)–(d) Drop casting of LMWG **1** in different RH leads to variation of pore size caused by the breath figure effect. A set of coatings comprising four different pore sizes was obtained. The micrographs depict native coatings (left) and irradiated coatings (right) at 5× magnification (top) and 20× magnification (bottom) respectively. The native coatings are colourless, while the topochemically polymerised coatings are red. The pore size is unaffected by the polymerisation. (e) Diacetylene **1** is an effective LMWG in a range of different solvents, from left to right: toluene, 1 : 1-mixture of cyclohexane and chloroform, diethyl ether, trifluoromethyl benzene, chloroform. The gels are slightly discoloured due to minor polymerisation under ambient conditions. (f) Relation between RH and average pore size of the coatings, blue: native coatings, magenta: irradiated coatings.

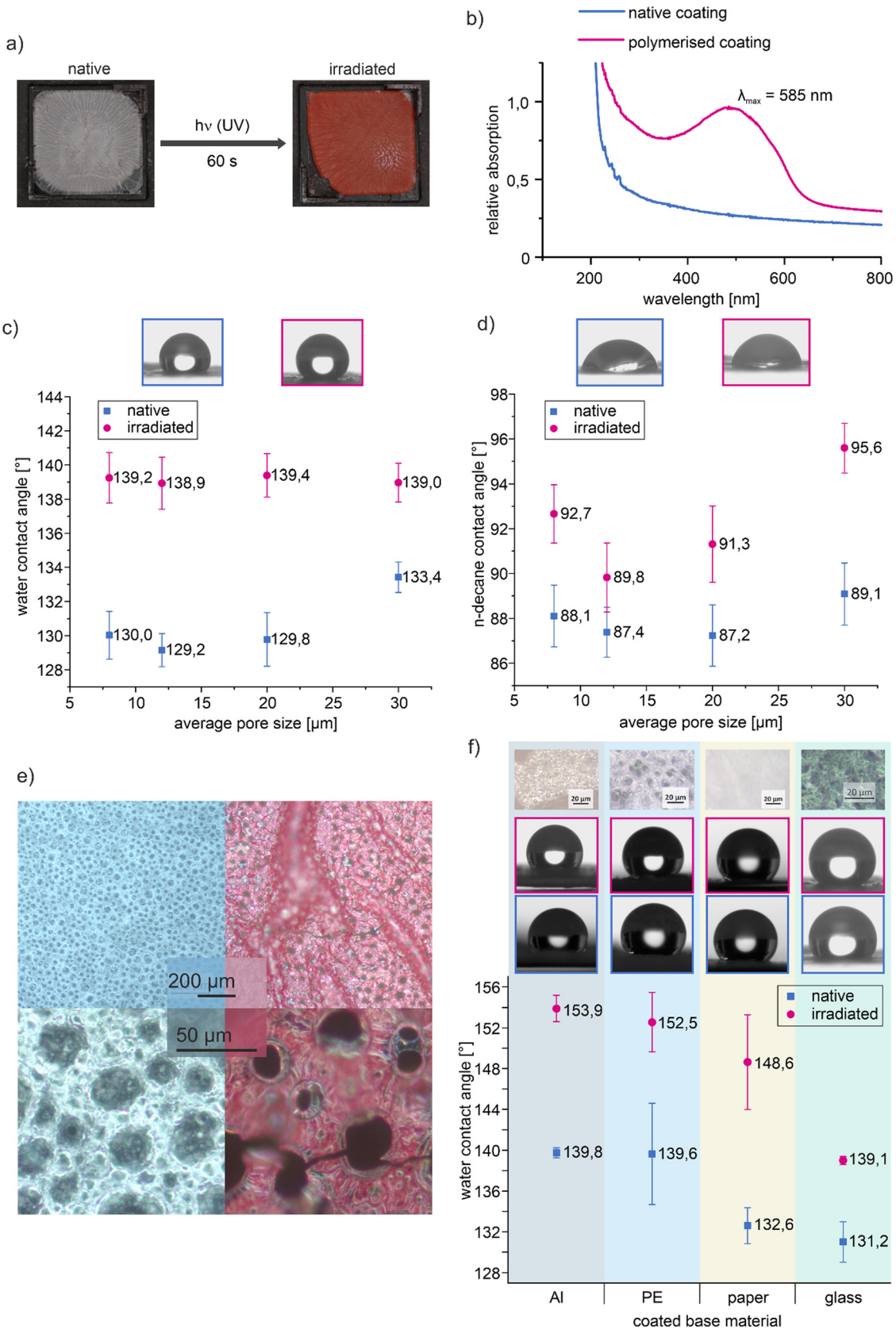

Fig. 3 (a) Appearance change of the coatings upon topochemical polymerisation initiated by UV-irradiation for 1 min. (b) UV-vis-spectrum of a dried film of LMWG **1** before (blue) and after UV-irradiation (magenta). (c) Static ^{H_2O}CA and (d) ^{dec}CA of coatings comprising different pore sizes before (blue) and after (magenta) UV-irradiation. (e) Minor crack formation during the photopolymerisation enhances the contact angles without impacting the mechanical integrity of the coatings (f) application of the coating on different base materials with the respective morphology (top) and the static ^{H_2O}CA (bottom) before (blue) and after (magenta) irradiation.

glass slide is broken in halves, optical microscopy of the edge reveals the coatings to consist of a single layer of pores (Fig. S3e, ESI†).

Water droplets adhere to surfaces tilted even by 180° (Fig. S3a–d, ESI†). Consequently, the coatings of LMWG **1** exhibit the rose petal effect rather than the lotus effect. This suggests the Wenzel mode of surface wetting to be prevalent.

2.2.3. Application of the coating on different base materials. To show the versatile aplicability of the coating, different base materials were coated and the hydrophobicities of the native and irradiated coatings were compared (Fig. 3f). The samples were prepared in RH = 81% because the glass-based samples were most evenly covered at this RH. As expected, coatings on paper show vastly different morphology compared to those on the liquid-impermeable base materials Al, PE or glass. The BFE is only present on the impermeable bases. However, the pore sizes differ from each other rather drastically due to different heat capacities as well as thermal conductivities of the base materials. This can clearly been seen on the Al-based sample which has much smaller pore diameters than the coatings on glass or PE. Because the Al allows for much faster heat transport, the evaporation leads to quicker cooling of the sample. Faster cooling leads to earlier gelation as well as suppression of coalescence, thus resulting in the formation of many small pores rather than larger ones. The paper however is completely soaked with the gelator sol and thus the cellulose fibres get impregnated by the waxy fluorous material. The additional roughness of the fibrous paper network leads to drastically enhanced ^{H_2O}CA of 140 ± 2° on paper compared to only 131 ± 2° on glass. Upon irradiation the ^{H_2O}CA are again increased by approximately 10% in all cases.

2.2.4. Mechanical stability of the coatings

2.2.4.1. Quantification of the mechanical stability. We initially probed the mechanical properties of the coatings by flushing the coated surfaces with sand (Fig. S7, ESI†). The areas of removed material on postflush samples were compared to the preflush samples by image analysis using imageJ (Fig. S6 and Table S1, ESI†). The relative stability trend of coatings obtained from different solvents was illucidated by this method, clearly marking chloroform as the superior solvent for the remaining study. However the image analysis reaches its limits when irradiated red surfaces are to be compared with colourless non-irradiated surfaces. Additionally we wanted to create a method to obtain an absolute measure for the coating strength instead of the relative information obtained from the sand flushing method. Thus we devised a reprioducible test to asses the mechanical robustness of the coatings using a home built device called the 'scratch balance'.[2]

The scratch balance allows us to reproducibly scratch coatings with a needle by applying a constant and adjustable force. The coated substrate is placed onto a platform, which pulls the substrate with constant velocity underneath a pivoted needle. The downward force exerted on the coating by the needle tip is adjusted by a pulley attached to the opposite end of the pivoted needle (Fig. 4a). The correlation between the input weights added to the pulley system and the downward force is calibrated by placing the needle onto a fine balance and recording the subsequent output displayed by the balance. The resulting calibration curve is depicted in Fig. S5 (ESI†).

This method yields a quantitative readout for the macroscopic coating stability in the following way: The applied downward force is varied stepwise and the resulting scratches are characterised by light microscopy. A rather low downward force results in little to no removal of material in the path of the needle, a sufficiently high downward force results in complete abrasion of the material in the needle's path. We chose to characterise the surfaces by the minimum downward force that is required to remove at least 90% of the material in the path of the needle (Fig. 4b and c). This coating-specific property will be referred to as 'critical downward force' $^{crit}F_{\downarrow}$. The threshold of 90% was selected because of the simpler recognisability of the almost complete scratch. Complete removal is not suitable as a criterion, as any force larger than the critical downward force would give the same result.[2] The input weight m_{in} within the basket of the scratch balance is increased stepwise by 0.1 g (equivalent to 0.44 mN), leading to an increasing downward force $F_{\downarrow}$ between the needle-tip and the coating (eqn (1) and (2)).

$$m_{out} = 0.45 \cdot m_{in} + m_0 = 0.45 \cdot m_{in} + 0.54\ g \quad (1)$$

$$F_{\downarrow} = m_{out} \cdot G \quad (2)$$

The resulting weight m_{out} is transmitted by the pulley system onto the needle tip. It can be calculated from the linear fit of the calibration curve (Fig. S5, ESI†) using eqn (1), with the input weight m_{in} as parameter and the system constant m_0. The downward force $F_{\downarrow}$ is obtained as product of m_{out} with the gravitational constant G using eqn (2). This way the critical downward force $^{crit}F_{\downarrow}$ is approached from below and obtained as the lowest readout that surpasses the threshold of 90% removed material within the scratch.

2.2.4.2. Mechanical properties of the native coatings. The critical downward forces $^{crit}F_{\downarrow}$ of irradiated and non-irradiated coatings are plotted against the respective pore size obtained through the breath figure effect (Fig. 4d). A clear trend between scratching stability and pore size is observed. Smaller pores yield a more compact and thus more stable coating – for the native coatings, breath figure arrays of 7 μm require 30 ± 4 mN, those of 12 μm 24 ± 2 mN, those with 20 μm pores 19 ± 1 mN, and arrays of 30 μm pores 13 ± 4 mN. This represents a drastic, more than two fold increase in stability from 30 μm to 7 μm pores, demonstrating that the mechanical properties of the coatings can be controlled within a broad range by the breath figure effect. An intuitive explanation for this behaviour is the weaker arch support effect as well as the thinner walls of larger pores leading to a more brittle and easily removable coating as compared to coatings with smaller pores.

2.2.4.3. Mechanical properties of the irradiated coatings. With the photoinduced topochemical polymerisation of LMWG **1**, the mechanical stability of the coatings is significantly increased (Fig. 4d). The most dramatic stability increase is observed for

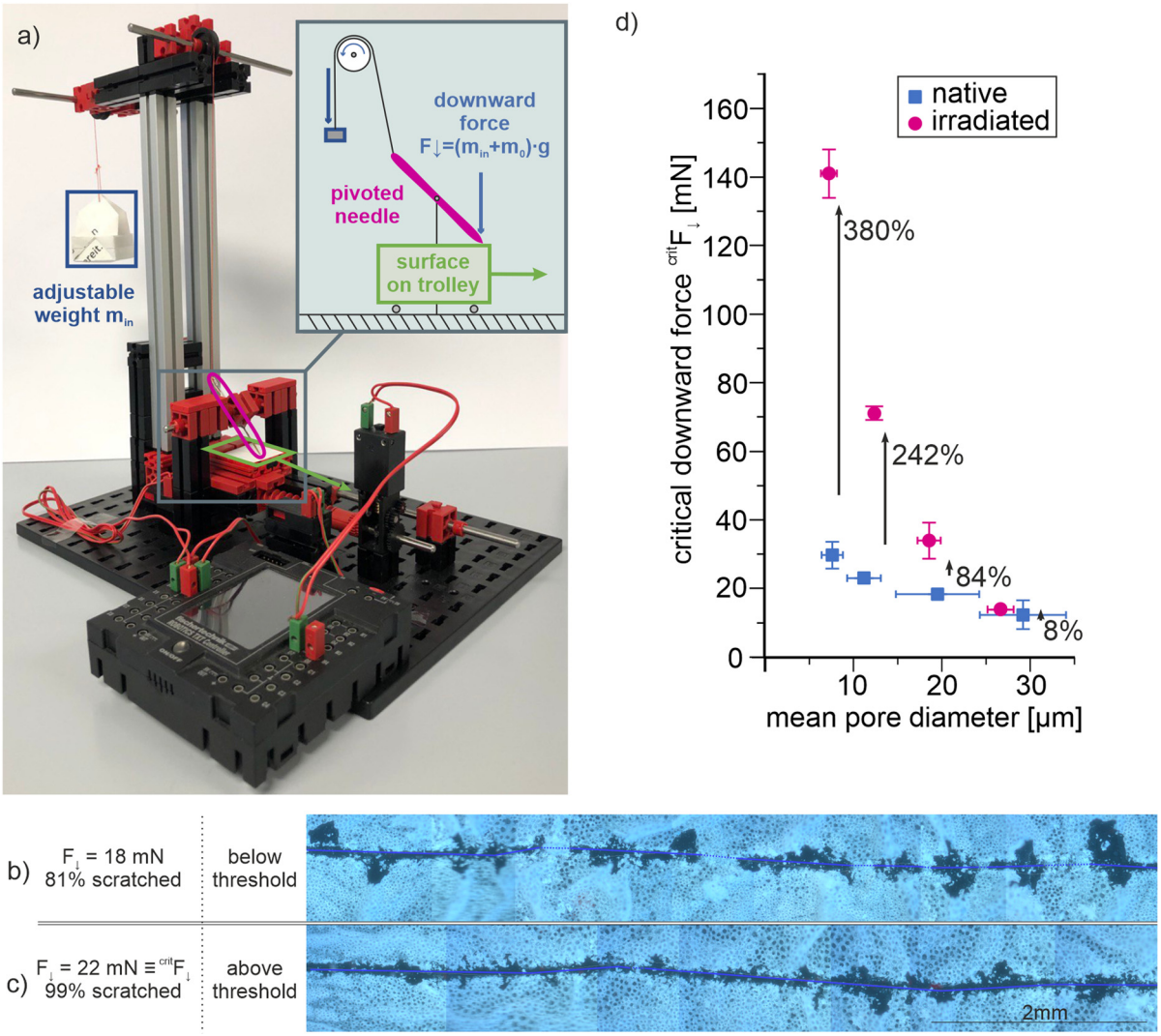

Fig. 4 (a) Setup of the scratch balance: coated samples are placed onto the platform underneath the still stationary needle. Weights are added to the basket attached to the pulley system, exerting a constant downward force $F_{\downarrow}$ from the needle tip onto the coating. The platform, which is controlled by a ROBO-TX-automation-robot-setup from Fischertechnik, subsequently translates with constant speed to create a scratch in the coating. (b) A scratch with insufficient $F_{\downarrow} < {}^{crit}F_{\downarrow}$ (below threshold) and (c) a scratch with sufficient $F_{\downarrow} \geq {}^{crit}F_{\downarrow}$ (above threshold). (d) The relation of the critical downward forces to the pore size.

coatings with smaller pores. Irradiated coatings with 7 µm pore diameter display a ${}^{crit}F_{\downarrow} = 144 \pm 7$ mN – an increase by 380% compared to the ${}^{crit}F_{\downarrow}$ of native coatings with the same pore size. For pore sizes of 12 µm an increase to ${}^{crit}F_{\downarrow} = 72 \pm 2$ mN (240%), for 20 µm pores to ${}^{crit}F_{\downarrow} = 35 \pm 5$ mN (84%), and for 30 µm to ${}^{crit}F_{\downarrow} = 14 \pm 2$ mN (8%) is observed. The irradiation thus significantly alters the intrinsic mechanical properties of the material. This is most notable in coatings with small pores, while the added mechanical stability of the coatings is much smaller for coatings with larger pores. This indicates that the mechanical properties of the coatings are dominated by the intrinsic material properties in more compact layers, whilst the impact of these intrinsic properties is lost in the larger pored coatings. By simply applying the coating under different ambient conditions, its mechanical properties can noticeably be tuned by the breath figure effect.

3. Conclusions

A novel fluorous LMWG was prepared in gram scale and applied to glass slides by drop casting, forming an omniphobic, rose-petal-like surface coating with ${}^{H_2O}CA = 131 \pm 2°$ and ${}^{dec}CA = 88 \pm 1°$. The coatings display breath figure arrays, their average pore size can be controlled by casting in different relative humidities. The dried coatings are either investigated as native coatings or irradiated to initiate topochemical polymerisation of the diacetylene core, providing red polymerised coatings. While the morphology of the coatings is preserved, the supramolecular diacetylene network is transformed into a covalently linked polydiacetylene. The photopolymerization leads to a significantly improved omniphobicity.

The applicability of our coating on different base-materials was demonstrated. The irradiated samples on Al and PE reach superhydrophobicity. We believe that the ability to impregnate

paper with LMWG **1** offers highly interesting applications as smart ink or for lithografic microchannel production. A sample of the impregnated omniphobic paper could be irradiated using a mask imprinting patterns of PDA onto it, while leaving the masked areas in the native state. Subsequent rinsing with chloroform would remove the native gelator while leaving the insoluble PDA thus potentially giving rise to printable omniphobic areas.

A home-built scratch balance for assessing the mechanical stability of thick film coatings allows us to reliably characterise and compare their mechanical properties. The coatings display a dependence of their mechanical stability on their pore size, which can conveniently be adjusted by the breath figure effect. Coatings comprising smaller pores are mechanically more stable. The mechanical stability is drastically enhanced by the topochemical polymerisation with the extent of the stabilising effect depending on the pore size. Smaller pores provide up to 380% more robust coatings after irradiation.

The intriguing properties and simple preparation of diacetylene-based coatings reported here seem promising to further investigate the influence of spacer length and ponytail structure on the resulting coating morphology and mechanical properties.

The successful implementation of topochemical polymerisation of a diacetylene-based LMWG coating is a promising step towards more mechanically robust self-assembled coatings. The diversity of features and enhanced properties, in combination with the extremely facile fabrication of these coatings, unfolds a range of potential applications based on diacetylene LMWG as coating material. The creation of hierarchical micro-nanostructures and subsequent topochemical hardening is of high value for the creation of smart coatings. The facile fixation of the hierarchical morphology by supramolecular polymerisation yields a mechanically robust omniphiobic coating without the need for complicated structuring techniques.

Author contributions

Conceptualization, methodology, writing – original draft preparation, visualization, formal analysis, data curation, Janos Wasternack.; investigation, Janos Wasternack and Tom White; writing – review and editing, Janos Wasternack, Tom White, Sebastian Müller and Christoph A. Schalley; supervision, project administration, funding acquisition, resources, Christoph A. Schalley; all authors have read and agreed to the published version of the manuscript.

Conflicts of interest

There are no conflicts to declare.

Acknowledgements

This work was supported by the SFB1349 ''Fluorine-Specific Interactions''. We would like to thank Tuğrul Kaynak for performing SEM measurements.

Notes and references

1 B. Bhushan, Y. C. Jung and M. Nosonovsky, in *Springer handbook of nanotechnology*, ed. B. Bhushan, Springer, Berlin, 3rd edn, 2010, pp. 1437–1524.
2 T. Darmanin and F. Guittard, Superhydrophobic and superoleophobic properties in nature, *Mater. Today*, 2015, **18**, 273–285.
3 P. Fratzl, J. Dunlop and R. Weinkamer, *Materials design inspired by nature. Function through inner architecture*, RSC Publishing, Cambridge, 2013.
4 T. V. Varghese, International Conference on Nanoscience, Engineering and Technology (ICONSET 2011), 2011, pp. 472–477.
5 H. Ye, L. Zhu, W. Li, H. Liu and H. Chen, Simple spray deposition of a water-based superhydrophobic coating with high stability for flexible applications, *J. Mater. Chem. A*, 2017, **5**, 9882–9890.
6 L. Zhou, S. Xu, G. Zhang, D. Cai and Z. Wu, A facile approach to fabricate self-cleaning paint, *Appl. Clay Sci.*, 2016, **132–133**, 290–295.
7 S. M. Imani, R. Maclachlan, K. Rachwalski, Y. Chan, B. Lee, M. McInnes, K. Grandfield, E. D. Brown, T. F. Didar and L. Soleymani, Flexible Hierarchical Wraps Repel Drug-Resistant Gram-negative and Positive Bacteria, *ACS Nano*, 2020, **14**, 454–465.
8 N. J. Shirtcliffe, G. McHale, S. Atherton and M. I. Newton, An introduction to superhydrophobicity, *Adv. Colloid Interface Sci.*, 2010, **161**, 124–138.
9 D. P. Curran, I. T. Horváth and J. A. Gladysz, *Handbook of fluorous chemistry*, Wiley-VCH, Weinheim, 2004.
10 J. Zhang, J. Li and Y. Han, Superhydrophobic PTFE Surfaces by Extension, *Macromol. Rapid Commun.*, 2004, **25**, 1105–1108.
11 M. E. Diaz, M. D. Savage and R. L. Cerro, The effect of temperature on contact angles and wetting transitions for *n*-alkanes on PTFE, *J. Colloid Interface Sci.*, 2017, **503**, 159–167.
12 C. W. Extrand, Modeling of Ultralyophobicity: Suspension of Liquid Drops by a Single Asperity, *Langmuir*, 2005, **21**, 10370–10374.
13 E. Huovinen, J. Hirvi, M. Suvanto and T. A. Pakkanen, Micro–Micro Hierarchy Replacing Micro–Nano Hierarchy: A Precisely Controlled Way To Produce Wear-Resistant Superhydrophobic Polymer Surfaces, *Langmuir*, 2012, **28**, 14747–14755.
14 Y. Fujisawa, A. Asano, Y. Itoh and T. Aida, Mechanically Robust, Self-Healable Polymers Usable under High Humidity: Humidity-Tolerant Noncovalent Cross-Linking Strategy, *J. Am. Chem. Soc.*, 2021, **143**, 15279–15285.
15 E. Huovinen, J. Hirvi, M. Suvanto and T. A. Pakkanen, Micro-micro hierarchy replacing micro-nano hierarchy: a precisely controlled way to produce wear-resistant superhydrophobic polymer surfaces, *Langmuir*, 2012, **28**, 14747–14755.
16 H. Ye, L. Zhu, W. Li, H. Liu and H. Chen, Simple spray deposition of a water-based superhydrophobic coating with high stability for flexible applications, *J. Mater. Chem. A*, 2017, **5**, 9882–9890.

17 P.-W. Lee, T. Kaynak, D. Al-Sabbagh, F. Emmerling and C. A. Schalley, Effect of Perfluorinated Side-Chain Length on the Morphology, Hydrophobicity, and Stability of Xerogel Coatings, *Langmuir*, 2021, **37**, 14390–14397.
18 Q. Wei, C. Schlaich, S. Prévost, A. Schulz, C. Böttcher, M. Gradzielski, Z. Qi, R. Haag and C. A. Schalley, Supramolecular Polymers as Surface Coatings: Rapid Fabrication of Healable Superhydrophobic and Slippery Surfaces, *Adv. Mater.*, 2014, **26**, 7358–7364.
19 E.-M. Schön, E. Marqués-López, R. P. Herrera, C. Alemán and D. Díaz Díaz, Exploiting molecular self-assembly: from urea-based organocatalysts to multifunctional supramolecular gels, *Chem. – Eur. J.*, 2014, **20**, 10720–10731.
20 M. Poddighe and P. Innocenzi, Hydrophobic Thin Films from Sol–Gel Processing: A Critical Review, *Materials*, 2021, **14**, 6799.
21 J. Sautaux, F. Marx, I. Gunkel, C. Weder and S. Schrettl, Mechanically robust supramolecular polymer co-assemblies, *Nat. Commun.*, 2022, **13**, 356.
22 M.-H. Zhang, C.-H. Li and J.-L. Zuo, A Supramolecular Polymer Formed by Small Molecules, *Cell Rep. Phys. Sci.*, 2020, **1**, 100144.
23 X. Dai, Y. Zhang, L. Gao, T. Bai, W. Wang, Y. Cui and W. Liu, A Mechanically Strong, Highly Stable, Thermoplastic, and Self-Healable Supramolecular Polymer Hydrogel, *Adv. Mater.*, 2015, **27**, 3566–3571.
24 K. Aoki, M. Kudo and N. Tamaoki, Novel odd/even effect of alkylene chain length on the photopolymerizability of organogelators, *Org. Lett.*, 2004, **6**, 4009–4012.
25 R. R. Chance and G. N. Patel, Solid-state polymerization of a diacetylene crystal: Thermal, ultraviolet, and γ-ray polymerization of 2,4-hexadiyne-1,6-diol bis-(p-toluene sulfonate), *J. Polym. Sci., Polym. Phys. Ed.*, 1978, **16**, 859–881.
26 S. M. Curtis, N. Le, T. Nguyen, X. Ouyang, T. Tran, F. W. Fowler and J. W. Lauher, What have We Learned about Topochemical Diacetylene Polymerizations?, *Supramol. Chem.*, 2005, **17**, 31–36.
27 N. Fujita, Y. Sakamoto, M. Shirakawa, M. Ojima, A. Fujii, M. Ozaki and S. Shinkai, Polydiacetylene nanofibers created in low-molecular-weight gels by post modification: control of blue and red phases by the odd–even effect in alkyl chains, *J. Am. Chem. Soc.*, 2007, **129**, 4134–4135.
28 V. Haridas, Y. K. Sharma, R. Creasey, S. Sahu, C. T. Gibson and N. H. Voelcker, Gelation and topochemical polymerization of peptide dendrimers, *New J. Chem.*, 2011, **35**, 303–309.
29 V. Kohlschütter, Über Disperses Aluminiumhydroxyd I, *Z. Anorg. Allg. Chem.*, 1919, **105**, 1–25.
30 T. Odani, S. Okada, C. Kabuto, T. Kimura, S. Shimada, H. Matsuda, H. Oikawa, A. Matsumoto and H. Nakanishi, Solid-State Reactions of Crystals Containing Two Kinds of Polymerizable Moieties of Diene and Diyne, *Cryst. Growth Des.*, 2009, **9**, 3481–3487.
31 O. J. Dautel, M. Robitzer, J.-P. Lère-Porte, F. Serein-Spirau and J. J. E. Moreau, Self-organized ureido substituted diacetylenic organogel. Photopolymerization of one-dimensional supramolecular assemblies to give conjugated nanofibers, *J. Am. Chem. Soc.*, 2006, **128**, 16213–16223.
32 K. Inoue, Y. Ono, Y. Kanekiyo, K. Hanabusa and S. Shinkai, Preparation of New Robust Organic Gels by *in situ* Cross-link of a Bis(diacetylene) Gelator, *Chem. Lett.*, 1999, 429–430.
33 D.-Y. Kim, S.-A. Lee, D. Jung, J. Koo, J. Soo Kim, Y.-T. Yu, C.-R. Lee and K.-U. Jeong, Topochemical polymerization of dumbbell-shaped diacetylene monomers: relationship between chemical structure, molecular packing structure, and gelation property, *Soft Matter*, 2017, **13**, 5759–5766.
34 H. Sixl, Spectroscopy of the intermediate states of the solid state polymerization reaction in diacetylene crystals, in *Polydiacetylenes*, ed. H.-J. Cantow, Springer, Berlin, Heidelberg, 1984, pp. 49–90.
35 H. Wang, F. Sun, C. Wang, Y. Zhu and H. Wang, A simple drop-casting approach to fabricate the super-hydrophobic PMMA-PSF-CNFs composite coating with heat-, wear- and corrosion-resistant properties, *Colloid Polym. Sci.*, 2016, **294**, 303–309.
36 K. Biradha and R. Santra, Crystal engineering of topochemical solid state reactions, *Chem. Soc. Rev.*, 2013, **42**, 950–967.
37 Y. Lifshitz, Y. Golan, O. Konovalov and A. Berman, Structural transitions in polydiacetylene Langmuir films, *Langmuir*, 2009, **25**, 4469–4477.
38 Z. Iqbal, N. S. Murthy, Y. P. Khanna, J. S. Szobota, R. A. Dalterio and F. J. Owens, The mechanism of the solid state phase transitions in the polydiacetylene, poly-4BCMU: thermal, X-ray diffraction and Raman scattering studies, *J. Phys. C: Solid State Phys.*, 1987, **20**, 4283–4295.
39 R. H. Baughman, Solid-state polymerization of diacetylenes, *J. Appl. Phys.*, 1972, **43**, 4362–4370.
40 R. Filler, J. F. O'Brien, J. V. Fenner and M. Hauptschein, Fluorinated Esters. II. Diesters of Perfluorocarboxylic Acids with Alcohols and Glycols, *J. Am. Chem. Soc.*, 1953, **75**, 966–968.
41 P. Kirsch, *Modern Fluoroorganic Chemistry*, Wiley-VCH, Weinheim, 2013.
42 N. Mureau, F. Guittard and S. Géribaldi, Convenient synthesis of thiols and disulfides in the polyfluorinated series incorporating a butylic spacer, *Tetrahedron Lett.*, 2000, **41**, 2885–2889.
43 P. Lucas, M. A. Jouani, H. Trabelsi and A. Cambon, Nouveaux procédés de préparation des isocyanates F-alkylés linéaires ou ramifiés à partir des iodures de 2-F-alkyléthyle, *J. Fluorine Chem.*, 1998, **92**, 17–22.
44 U. H. F. Bunz, Breath Figures as a Dynamic Templating Method for Polymers and Nanomaterials, *Adv. Mater.*, 2006, **18**, 973–989.
45 M. B. Avinash, E. Verheggen, C. Schmuck and T. Govindaraju, Self-cleaning functional molecular materials, *Angew. Chem., Int. Ed.*, 2012, **51**, 10324–10328.
46 M. Liu, X. Zhang, D. Wang, J. Cheng, X. Pang, W. Qu, C. Li and S. Li, Facile Fabrication of Superhydrophobic Surface from Fluorinated POSS Acrylate Copolymer *via* One-Step Breath Figure Method and Its Anti-Corrosion Property, *Polymers*, 2019, **11**, 1953.
47 H. Yabu, Fabrication of honeycomb films by the breath figure technique and their applications, *Sci. Technol. Adv. Mater.*, 2018, **19**, 802–822.

48 J.-S. Poh, S. Makai, T. von Keutz, D. N. Tran, C. Battilocchio, P. Pasau and S. V. Ley, Rapid Asymmetric Synthesis of Disubstituted Allenes by Coupling of Flow-Generated Diazo Compounds and Propargylated Amines, *Angew. Chem., Int. Ed.*, 2017, **56**, 1864–1868.
49 D. Crich, K. Ranganathan and X. Huang, Generation and reaction of alkene radical cations under nonoxidizing conditions: synthesis of the pyrrolizidine nucleus, *Org. Lett.*, 2001, **3**, 1917–1919.
50 C. Glaser, Beiträge zur Kenntniss des Acetenylbenzols, *Ber. Dtsch. Chem. Ges.*, 1869, **2**, 422–424.
51 P. Siemsen, R. C. Livingston and F. Diederich, Acetylenic Coupling: A Powerful Tool in Molecular Construction, *Angew. Chem., Int. Ed.*, 2000, **39**, 2632–2657.
52 D. Mampallil and H. B. Eral, A review on suppression and utilization of the coffee-ring effect, *Adv. Colloid Interface Sci.*, 2018, **252**, 38–54.
53 T. G. Dane, J. E. Bartenstein, B. Sironi, B. M. Mills, O. Alexander Bell, J. Emyr Macdonald, T. Arnold, C. F. J. Faul and W. H. Briscoe, Influence of solvent polarity on the structure of drop-cast electroactive tetra(aniline)-surfactant thin films, *Phys. Chem. Chem. Phys.*, 2016, **18**, 24498–24505.
54 H. Bai, C. Du, A. Zhang and L. Li, Breath figure arrays: unconventional fabrications, functionalizations, and applications, *Angew. Chem., Int. Ed.*, 2013, **52**, 12240–12255.
55 U. H. F. Bunz, Breath Figures as a Dynamic Templating Method for Polymers and Nanomaterials, *Adv. Mater.*, 2006, **18**, 973–989.
56 H. Ma and J. Hao, Ordered patterns and structures *via* interfacial self-assembly: superlattices, honeycomb structures and coffee rings, *Chem. Soc. Rev.*, 2011, **40**, 5457–5471.
57 Y. Zhang and Z. Li, Formation of Hierarchical Porous Structure *via* Breath Figure Method, *Adv. Condens. Matter Phys.*, 2018, **2018**, 1–6.